Electronic Supplementary Material (ESI) for New Journal of Chemistry.
This journal is © The Royal Society of Chemistry and the Centre National de la Recherche Scientifique 2022

Experimental Section

Synthesis of Ir/RGO

All chemical reagents were of analytical grade from commercial sources and were not purified during use. As depicted in Fig. 1a, Ir/RGO was prepared by a one-pot hydrothermal process assisted by the microwave treatment. Briefly, 50 mg of graphene oxide (GO) was firstly dispersed in distilled water under ultrasonication for 1 h, followed by adding 10 mg of $IrCl_3 \cdot 3H_2O$ under ultrasonication for another 10 min. Afterwards, the mixed solutions were sealed into a quartz tube, which were reacted for 15 min under microwave irradiation (2450 MHz). Afterwards, the precipitates were collected through centrifuging, washing with deionized water/ethanol, and drying under vacuum.

Electrochemical experiments

All the electrochemical performance measurements were carried out using a CHI-760E electrochemical workstation (CH Instrument Inc.) at room temperature. In a three-electrode system, Ag/AgCl (saturated KCl), graphite rod and as-prepared carbon cloth (CC) sample were used as reference, counter and working electrodes, respectively. All potentials were converted to the reversible hydrogen electrode (RHE) scale according to: E_{RHE} (V)=$E_{Ag/AgCl}$+0.197+0.059×pH. The working electrodes were fabricated by drop-casting 20 μL of catalyst ink onto carbon paper to achieve a loading density of 0.2 mg·cm^{-2}. The catalyst ink was prepared by dispersing 1 mg of the catalysts in 100 μL of ethyl alcohol containing 5 μL of Nafion (5 wt%) under ultrasonication. The NRR measurements were conducted in a two-compartment electrochemical H-cell separated with a proton exchange membrane (Nafion 211, Dupont). The Nafion membrane was pretreated by heating it in 5% H_2O_2 aqueous solution at 80 °C for 1 h and then in deionized water at 80 °C for another 1 h. Prior to NRR tests, all the feeding gases were purified through acid trap (0.05 M H_2SO_4) and alkaline trap (0.1 M KOH)) to remove any possible contaminants (NH_3 and NO_x). In the process of potentiostatic test, a flow of N_2 (99.999%) with a rate of 20 mL min^{-1} was continuously fed to the cathodic compartment. After NRR electrolysis at

specified potentials for 2 h, the produced NH_3 was quantitatively determined by the indophenol blue method[1], and the possible byproduct (N_2H_4) was determined by the method of Watt and Chrisp[2]. The detailed determination procedures are given in our previous publications[3-5].

Calculations of NH_3 yield and Faradaic efficiency

$$\mathrm{NH_3\ yield}\ (\mu \mathrm{g\ h^{-1}\ mg_{cat.}^{-1}}) = \frac{c_{\mathrm{NH_3}} \times V}{t \times m} \tag{1}$$

Faradaic efficiency was calculated by the following equation:

$$\text{Faradaic efficiency}\ (\%) = \frac{3 \times F \times c_{\mathrm{NH_3}} \times V}{17 \times Q} \times 100\% \tag{2}$$

where c_{NH3} (μg mL^{-1}) is the measured NH_3 concentration, V (mL) is the volume of the electrolyte, t (h) is the reduction time and m (mg) is the mass loading of the catalyst on CC. F (96500 C mol^{-1}) is the Faraday constant, Q (C) is the quantity of applied electricity.

Characterizations

Transmission electron microscopy (TEM), high-resolution transmission electron microscopy (HRTEM) and selected area electron diffraction (SAED) were carried out on a Tecnai G^2 F20 microscope. X-ray diffraction (XRD) pattern was conducted on a Rigaku D/max 2400 diffractometer. X-ray photoelectron spectroscopy (XPS) analysis was recorded on a PHI 5702 spectrometer. Dinitrogen temperature-programmed desorption (N_2-TPD) profiles were performed on a Chem-BET 3000 (Quantachrome) apparatus. The UV-vis absorbance measurements were performed using a MAPADA P5 spectrophotometer. 1H nuclear magnetic resonance (NRM) measurements were carried out on a 500 MHz Bruker superconducting-magnet NMR spectrometer.

Calculation details

All the density functional theory (DFT) calculations were conducted with Cambridge sequential total energy package (CASTEP). The Perdew-Burke-Ernzerhof (PBE) functional with the generalized gradient approximation (GGA) was used to assess exchange-correlation contributions and the DFT-D method was chosen to describe van der Waals (vdW) interactions. A kinetic energy cutoff of 580 eV was

used for the plane wave expansion. The k-point grid was set at 4 × 4 × 1 for surface calculations. The convergence threshold was set as 10^{-5} eV for total energy. The vacuum layers were larger than 15 Å above all the planes to avoid the unphysical interaction between periodic images.

The adsorption energy (ΔE) is defined as [6]

$$\Delta E = E_{\text{ads/slab}} - E_{\text{ads}} - E_{\text{slab}} \quad (3)$$

where $E_{\text{ads/slab}}$, E_{ads} and E_{slab} are the total energies for adsorbed species on slab, adsorbed species and isolated slab, respectively.

The Gibbs free energy (ΔG, 298 K) of reaction steps is calculated by [6]:

$$\Delta G = \Delta E + \Delta ZPE - T\Delta S \quad (4)$$

where ΔE is the adsorption energy, ΔZPE is the zero point energy difference and $T\Delta S$ is the entropy difference between the gas phase and adsorbed state. The entropies of free gases were acquired from the NIST database.

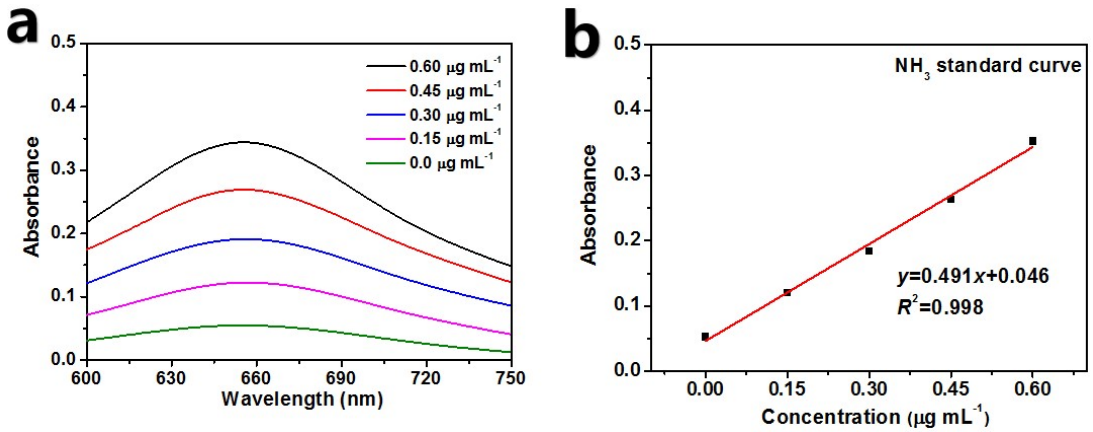

Fig. S1. (a) UV-vis absorption spectra of indophenol assays with NH_4Cl after incubated for 2 h at ambient conditions. (b) Calibration curve used for calculation of NH_3 concentrations.

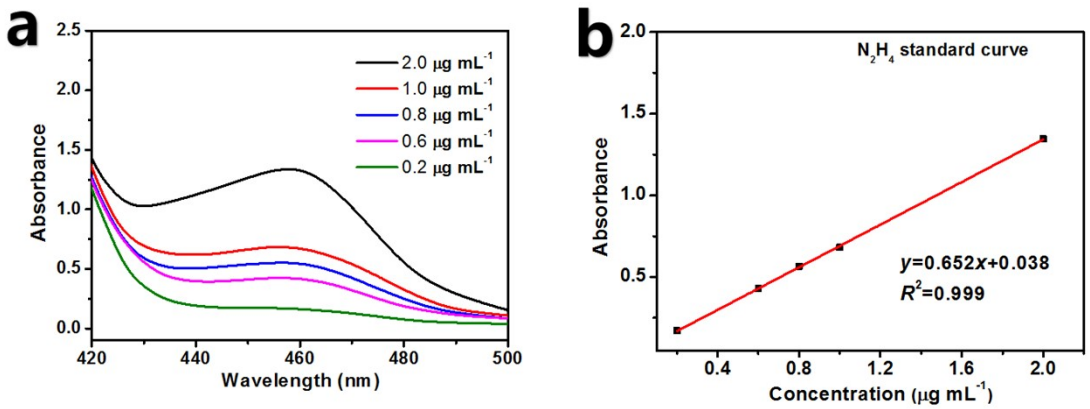

Fig. S2. (a) UV-vis absorption spectra of N_2H_4 assays after incubated for 20 min at ambient conditions. (b) Calibration curve used for calculation of N_2H_4 concentrations.

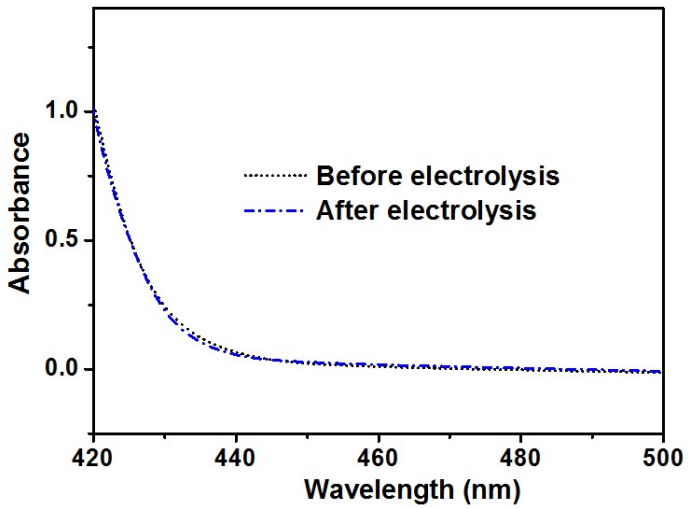

Fig. S3. UV-vis spectra of the electrolytes (stained with the chemical indicator based on the method of Watt and Chrisp) before and after 2 h of NRR electrolysis over Ir/RGO at -0.3 V.

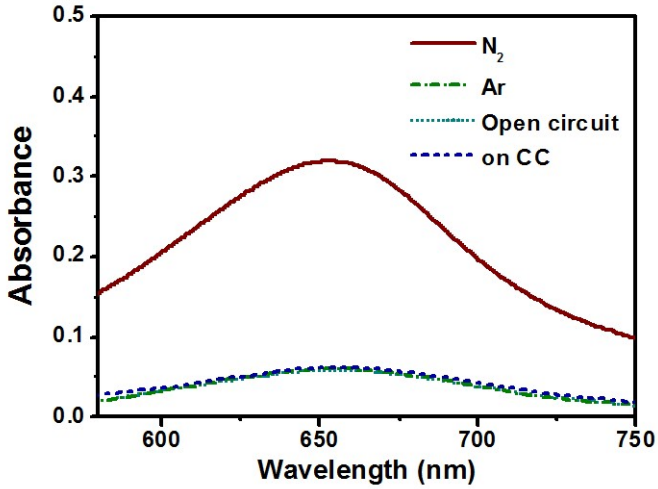

Fig. S4. UV-vis absorption spectra of working electrolytes after 2 h of electrolysis in Ar-saturated solutions on Ir/RGO at -0.3 V, N_2-saturated solution on Ir/RGO at open circuit, and N_2-saturated solution on pristine CC at -0.3 V.

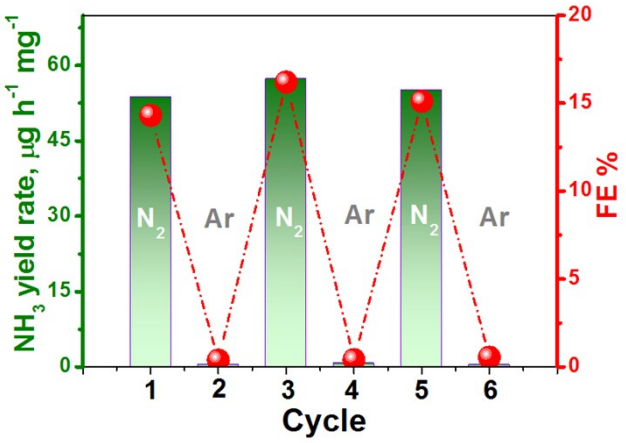

Fig. S5. Switching test in Ar- and N_2-saturated solution for NRR electrocatalysis over Ir/RGO at -0.3 V.

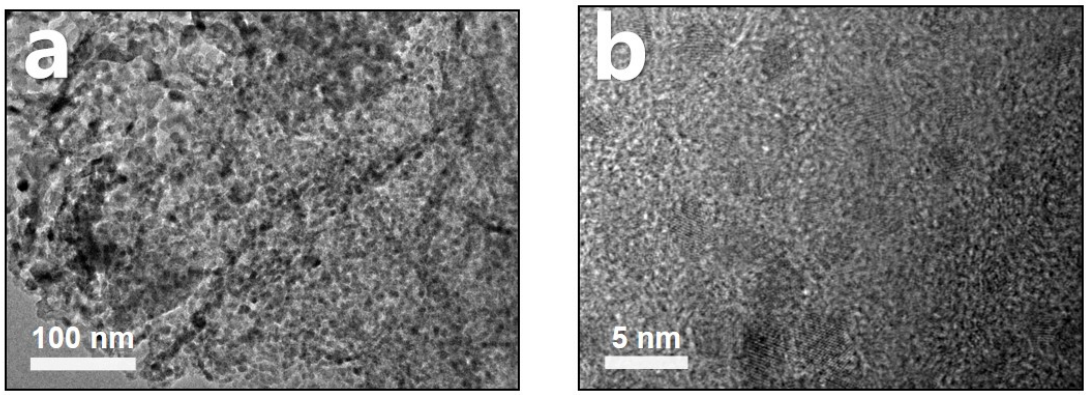

Fig. S6. (a) TEM and (b) HRTEM images of Ir/RGO after stability test.

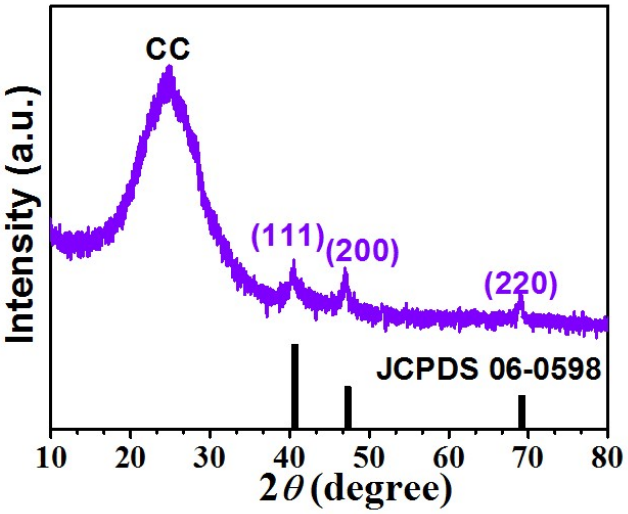

Fig. S7. XRD pattern of Ir/RGO after stability test.

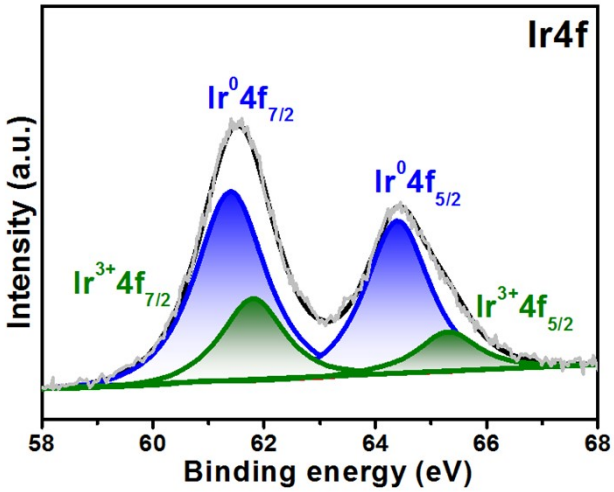

Fig. S8. XPS Ir4f spectrum of Ir/RGO after stability test.

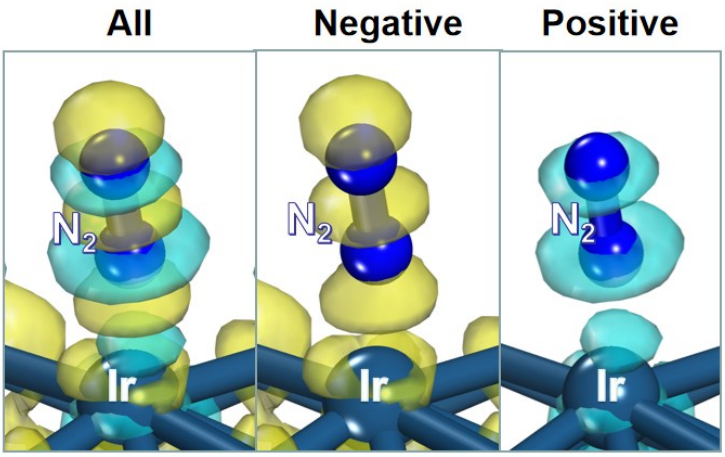

Fig. S9. Differential charge density of absorbed N_2 on Ir/RGO. Yellow and cyan iso-surfaces represent electron accumulation and electron depletion, respectively.

Table S1. Comparison of the optimum NH_3 yield and Faradic efficiency (FE) for the state-of-the-art NRR electrocatalysts at ambient conditions

Catalyst	Electrolyte	Potential (V vs RHE)	NH_3 yield rate ($\mu g\ h^{-1}\ mg^{-1}$)	FE (%)	Ref.
Mosaic Bi nanosheets	0.1 M Na_2SO_4	-0.8	13.23	10.46	[7]
Mo_2C/C	0.5 M Li_2SO_4	-0.3	11.3	7.8	[8]
Black phosphorus	0.01 M HCl	-0.7	31.37	5.07 (-0.6)	[9]
Au/CeO_x-RGO	0.1 M KOH	−0.2	8.31	10.1	[10]
Au-TiO_2 sub-nanocluster	0.1 M HCl	-0.2	21.4	8.11	[11]
B_4C nanosheet	0.1 M HCl	-0.75	26.57	15.95	[12]
Defect-rich MoS_2 nanoflower	0.1 M Na_2SO_4	-0.4	29.28	8.34	[13]
Sulfur-doped graphene	0.1 M HCl	-0.6	27.3	11.5 (-0.5V)	[14]
N-doped carbon spikes	0.25 M $LiClO_4$	-1.19	97.18	11.56	[15]
Mo single atoms	0.1 M KOH	-0.3	34	14.6	[16]
Fe−N/C hybrid	0.1 M KOH	-0.2	34.83	9.28	[17]
Ir/RGO	**0.5 M $LiClO_4$**	**-0.3**	**55.6**	**15.3**	**This wok**

Supplementary references

[1]. D. Zhu, L. Zhang, R. E. Ruther and R. J. Hamers, *Nat. Mater.*, 2013, **12**, 836.

[2]. G. W. Watt and J. D. Chrisp, *Anal. Chem.*, 1952, **24**, 2006-2008.

[3]. Q. Li, Y. Guo, Y. Tian, W. Liu and K. Chu, *J. Mater. Chem. A*, 2020, **8**, 16195-16202.

[4]. W. Gu, Y. Guo, Q. Li, Y. Tian and K. Chu, *ACS Appl. Mater. Inter.*, 2020, **12**, 37258-37264.

[5]. K. Chu, J. Wang, Y. P. Liu, Q. Q. Li and Y. L. Guo, *J. Mater. Chem. A*, 2020, **8**, 7117-7124.

[6]. A. A. Peterson, *Energy Environ. Sci.*, 2010, **3**, 1311-1315.

[7]. L. Li, C. Tang, B. Xia, H. Jin, Y. Zheng and S.-Z. Qiao, *ACS Catal.*, 2019, **9**, 2902-2908.

[8]. H. Cheng, L. X. Ding, G. F. Chen, L. Zhang, J. Xue and H. Wang, *Adv. Mater.*, 2018, **30**, 1803694.

[9]. L. L. Zhang, L. X. Ding, G. F. Chen, X. F. Yang and H. H. Wang, *Angew. Chem. Int. Edit.*, 2019, **131**, 2638-2642.

[10]. S. J. Li, D. Bao, M. M. Shi, B. R. Wulan, J. M. Yan and Q. Jiang, *Adv. Mater.*, 2017, **29**, 1700001.

[11]. M. M. Shi, D. Bao, B. R. Wulan, Y. H. Li, Y. F. Zhang, J. M. Yan and Q. Jiang, *Adv. Mater.*, 2017, **29**, 1606550.

[12]. W. Qiu, X.-Y. Xie, J. Qiu, W.-H. Fang, R. Liang, X. Ren, X. Ji, G. Cui, A. M. Asiri and G. Cui, *Nat. Commun.*, 2018, **9**, 3485.

[13]. X. Li, T. Li, Y. Ma, Q. Wei, W. Qiu, H. Guo, X. Shi, P. Zhang, A. M. Asiri and L. Chen, *Adv. Energy. Mater.*, 2018, **8**, 1801357.

[14]. L. Xia, J. Yang, H. Wang, R. Zhao, H. Chen, W. Fang, A. M. Asiri, F. Xie, G. Cui and X. Sun, *Chem. Commun.*, 2019, **55**, 3371-3374.

[15]. Y. Song, D. Johnson, R. Peng, D. K. Hensley, P. V. Bonnesen, L. Liang, J. Huang, F. Yang, F. Zhang and R. Qiao, *Sci. Adv.*, 2018, **4**, e1700336.

[16]. L. Han, X. Liu, J. Chen, R. Lin, H. Liu, F. Lu, S. Bak, Z. Liang, S. Zhao and E. Stavitski, *Angew. Chem. Int. Edit.*, 2018, **58**, 2321-2325.

[17]. Y. Wang, X. Cui, J. Zhao, G. Jia, L. Gu, Q. Zhang, L. Meng, Z. Shi, L. Zheng and C. Wang, *ACS Catal.*, 2018, **9**, 336-344.